Inviscid diffusion of vorticity in low-temperature superfluid helium

E. Rickinson, N. G. Parker, A. W. Baggaley, and C. F. Barenghi*
Joint Quantum Centre (JQC) Durham–Newcastle, School of Mathematics, Statistics and Physics, Newcastle University, Newcastle upon Tyne, NE1 7RU, United Kingdom

(Received 16 November 2018; revised manuscript received 10 May 2019; published 3 June 2019)

We numerically study the spatial spreading of quantized vortex lines in low-temperature liquid helium. The vortex lines, initially concentrated in a small region, diffuse into the surrounding vortex-free helium, a situation which is typical of many experiments. We find that this spreading, which occurs in the absence of viscosity, emerges from the interactions between the vortex lines and can be interpreted as a diffusion process with effective coefficient equal to approximately 0.5κ where κ is the quantum of circulation.

DOI: 10.1103/PhysRevB.99.224501

I. INTRODUCTION

The work which we describe is driven by the comparison [1] between turbulence in ordinary fluids (classical turbulence) and turbulence in superfluid helium (quantum turbulence). The main difference is the nature of the vorticity. In ordinary fluids, vorticity is a continuous field, and vortices have arbitrary shape and strength. In superfluid helium, quantum mechanics constrains the vorticity to individual vortex lines of atomic thickness (the vortex core radius is only $a_0 \approx 0.1$ nm) and fixed circulation $\kappa = h/m \approx 10^{-7}$ m^2/s (where h is Planck's constant and m is the mass of one ^{4}He atom). In superfluid helium, turbulence thus takes the form of a disordered tangle of interacting vortex lines. Moreover, at temperatures below around 1 K, thermal excitations are negligible and the vortex lines move in a perfect background fluid without viscosity.

Most experimental, theoretical, and numerical studies have addressed quantum turbulence in its simplest form: statistically steady, homogeneous, and isotropic. These studies have revealed similarities and differences with respect to ordinary turbulence, in terms of energy spectra [2–4], decay [5,6], intermittency [7–9], and velocity statistics [10–12]. Much less is known about turbulence which is inhomogeneous, in particular turbulence which is initially confined in a small region of space and is free to spread out. A better understanding of this diffusion problem would help to interpret many helium experiments in which ultrasound [13], oscillating spheres [14], wires, grids [15], and forks [16,17] create quantum turbulence in helium at rest, and from which the turbulence may spread and fill the experimental cell. Particularly important, as already remarked, is the low-temperature limit, in which the normal fluid is negligible and the dynamics of the vortex lines is simpler, at least in principle.

In this article we report the results of numerical simulations of the diffusion of a turbulent tangle of vortex lines which is initially localized in a region at the center of the computational domain. In the related context of two-dimensional (2D) trapped Bose–Einstein condensates, using the Gross–Pitaevskii equation (GPE) model, we found [18] that an initial vortex cluster diffuses via two distinct mechanisms: the evaporation of small vortex-antivortex pairs (vortex dipoles) which quickly leave the vortex cluster, and the slower spread of the cluster itself. The latter effect is like a classical diffusion process with an effective viscosity $\nu' \approx \kappa$.

The natural question which we address here is whether this effect holds true in three dimensions (3D) in the context of superfluid helium. The extra dimension introduces effects which are absent in 2D, such as vortex reconnections and Kelvin waves. A pioneering numerical study by Tsubota *et al.* [19] of the 3D diffusion of a vortex tangle reported a value of ν' smaller than what we found in 2D, albeit by a different approach and different initial conditions. These differences add further motivations to revisit the 3D diffusion problem.

II. METHODS

A. Evolution of the vortex tangle

To numerically simulate the evolution of a tangle of quantized vortex lines, we use the vortex filament method (VFM) of Schwarz [20], which is a more realistic model of turbulent He II than the GPE (which gives a good quantitative description of low-temperature Bose–Einstein condensates [21]). The VFM describes vortex lines as space curves $\mathbf{s}(\xi, t)$ (where t is time and ξ is arclength) which move according to the Biot–Savart law:

$$\frac{d\mathbf{s}}{dt} = -\frac{\kappa}{4\pi} \oint \frac{(\mathbf{s}-\mathbf{r}) \times d\mathbf{r}}{|\mathbf{s}-\mathbf{r}|^3}, \tag{1}$$

where the line integral extends over all vortex lines. Since there are no boundaries, all vortex lines form closed loops. Our VFM [11] uses a Lagrangian discretization along the vortex lines, with discretization points continuously added or removed to maintain the chosen spatial resolution of $\delta = 0.015$ cm. Vortex loops consisting of less than five discretization points are removed, modeling the effects of the small residual friction which is present even for $T < 1$ K. The Biot–Savart integral is de-singularized in a standard way [20] based on the vortex core cutoff a_0. The procedure for vortex

*carlo.barenghi@newcastle.ac.uk

 ©2019 American Physical Society

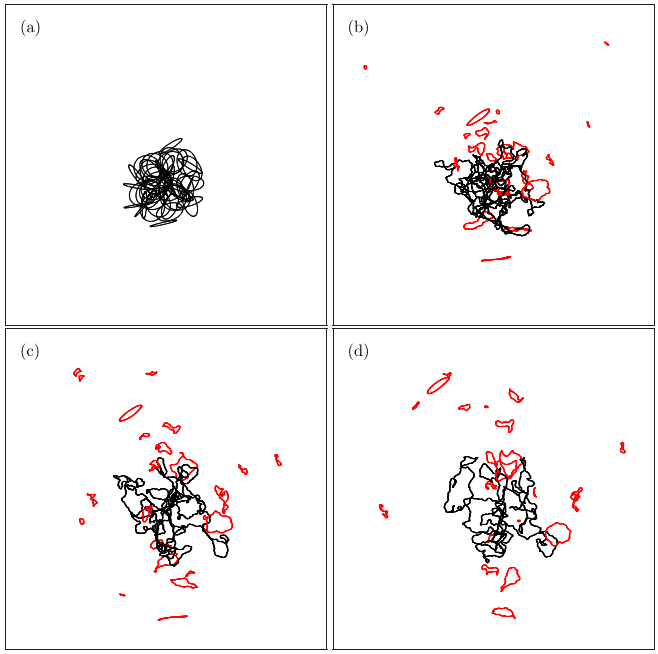

FIG. 1. Typical time evolution of the vortex tangle: (a) $t = 0$ s, (b) $t = 100$ s, (c) $t = 200$ s, and (d) $t = 300$ s. All panels show the region -2.5 cm $\leqslant x, y \leqslant 2.5$ cm projected onto the $z = 0$ plane. The computational domain is infinite (no boundaries). Note how the vortex tangle spreads out. Vortex loops containing fewer than 200 points are shown in red, with the remaining vortices shown in black.

reconnections is implemented algorithmically [20,22]. The resulting system of differential equations is integrated in time by using a third-order Adams–Bashforth scheme with a time step of 5×10^{-3} s.

The typical initial condition, shown in Fig. 1(a), consists of a set of randomly oriented vortex loops with radius 0.24 cm, randomly and independently translated in the x, y, and z directions according to a normal distribution with standard deviation 1 cm. To explore the effect of changing the initial vortex line density we perform two sets of simulations, one initialized with 50 vortex loops, leading to an initial vortex line density (vortex length per unit volume) of $L \sim 70$ cm^{-2} at the center of the infinite computational domain, and one using 100 vortex loops, with an initial vortex line density of $L \sim 140$ cm^{-2}.

B. Determining the effective diffusion

We estimate the effective diffusion of the vortex tangle by using two different techniques. The first technique follows the work of Tsubota *et al.* [19], who determined ν' by using the following modified Vinen equation for a space-dependent vortex line density $L(\mathbf{x}, t)$:

$$\frac{\partial L}{\partial t} = -\frac{\kappa}{2\pi}\chi_2 L^2 + \nu'\nabla^2 L. \tag{2}$$

The original Vinen equation [23] (see Appendix) balances a generation term (proportional to the driving counterflow velocity and $L^{3/2}$) against a decaying term (proportional to L^2). Equation (2) contains the same decaying term of the original Vinen equation (proportional to L^2) but lacks the generation term (because it is concerned with decay at zero temperature), and postulates the existence of a diffusion process represented by the new term $\nu'\nabla^2 L$; this new term turns the original Vinen equation into a parabolic partial differential equation. In writing Eq. (2), Tsubota *et al.* assumed that ν' depends on the temperature but is independent of the vortex line density. To determine ν', they fit the computed coarse-grained vortex line density to the numerical solution of Eq. (2). The fit, however, requires knowledge of Vinen's parameter χ_2. Tsubota *et al.* estimated [24] that $\chi_2 \approx 0.3$ from separate numerical simulations at $T = 0$ performed by using the local induction approximation to the exact Biot–Savart law [Eq. (1)]. Physically, in this zero-temperature limit, χ_2 models a sink of vortex lines due to the dissipation of kinetic energy through both vortex reconnections and phonon emission (induced by high-frequency Kelvin waves [25]).

It has been noted that χ_2 depends on the local vortex line density at finite temperatures [26]. We independently estimate values of χ_2 in the zero-temperature limit, using the full Biot–Savart law of Eq. (1), for 13 values of L, finding $\chi_2(L) \approx 0.07L^{0.4}$; this is detailed further in the Appendix. Assuming spherical symmetry, we then estimate $L(r)$ (where r is the radial distance from the center) by integrating over the vortex lines within spherical shells, subdividing the line segments for a more accurate measurement when they cross between shells, and dividing by the volume of these shells. We numerically solve the modified Vinen equation in a radially symmetric coordinate system, using fourth-order finite difference methods for spatial derivatives, and a third-order Adams–Bashforth time integration scheme with time step $\Delta t = 10^{-2}$ s. We use a reflective boundary condition to enforce $dL/dr = 0$ at $r = 0$, impose $L = 0$ at $r = 10$ cm (far from the region of interest), and use the initial vortex line density as a function of r estimated from our VFM simulations as the initial condition. The local value of χ_2 is taken to be $\chi_2(L) = 0.07L^{0.4}$ based on our estimates above.

The second technique is based on considering the deviation in the trajectories of diffusing tracers of the flow [27], which in our context is provided by the individual vortex discretization points modelled by the VFM. We know that the diffusion constant ν of a scalar field $F(x, y, z, t)$ which satisfies the diffusion equation

$$\frac{\partial F}{\partial t} = \nu\nabla^2 F, \tag{3}$$

is related to the root-mean-square (rms) deviation $d_{\mathrm{rms}}(t)$ by

$$\nu = \frac{d_{\mathrm{rms}}^2(t)}{4t}. \tag{4}$$

We define the rms deviation of our $N_0(t)$ vortex discretization points from their initial positions as

$$d_{\mathrm{rms}}(t) = \sqrt{\frac{1}{N_0(t)}\sum_{i=1}^{N_0(t)}\left[\Delta x_i^2(t) + \Delta y_i^2(t) + \Delta z_i^2(t)\right]}, \tag{5}$$

where $\Delta x_i(t) = x_i(t) - x_i(0)$, $\Delta y_i(t) = y_i(t) - y_i(0)$, and $\Delta z_i(t) = z_i(t) - z_i(0)$.

Using Eq. (4) we can define an effective 3D diffusion coefficient ν' representing the spatial spreading of the vortex cluster.

Because discretization points along vortex lines are continually removed and added to maintain the spatial resolution, care must be taken in establishing their trajectories. In most cases there is a direct link between a point at a given time and the same point at the previous time (the ancestor). If a point is newly inserted and thus lacks an ancestor at the previous time, we consider the ancestors of the discretization points on either side of the newly inserted point and store both these values as ancestors of the new point, using the average initial position of these ancestors as the initial position of the new point. This process is iterative as ancestors are concatenated in successive time steps. This second technique generalizes our previous 2D work [18] to 3D.

III. RESULTS

The typical evolution of the initial vortex rings into a turbulent vortex cluster is shown in Fig. 1. Before proceeding with the calculation of ν', a natural question arises: what is the character of this turbulence? Usually the answer is given in terms of the energy spectrum, but in this case the turbulence is neither steady nor homogeneous, and the interpretation of the spectrum would be difficult. We proceed differently and calculate the transverse velocity correlation function $f_\perp(r,t) = \langle v_\perp(\mathbf{x},t)v_\perp(\mathbf{x}+r\hat{\mathbf{e}}_\perp,t)\rangle/\langle v_\perp(\mathbf{x},t)^2\rangle$, and find that it rapidly decreases with distance, meaning that the turbulent velocity field is essentially random; at $t=0$, we find that $f_\perp(\ell/2,0)\approx 0.27$ only, where ℓ is the intervortex spacing, indicative of the Vinen (ultraquantum) regime of quantum turbulence [5], characterized by the absence of an energy cascade [4]. Similar turbulence and correlation functions have been predicted in trapped atomic Bose–Einstein condensates [28].

We now consider how the turbulence spreads in space. The initial vortex rings interact, become distorted, and undergo vortex reconnections, generating small vortex loops; if these small loops are in the outer part of the cluster and are oriented outwards, they quickly leave the cluster, as seen in the figure. This "vortex evaporation" [29] has been noticed in experiments [30] and reported in other 2D and 3D numerical simulations [18,31]. Here we concentrate on the slower spread of the main vortex cluster.

We first follow the approach of Tsubota *et al.* [19] and seek the solution of Eq. (2), estimating ν' by minimizing the sum of square errors between the vortex line density estimated from the VFM simulations and the numerical solution of Eq. (2). We find that, using this method, our estimate of ν' is very sensitive to the initial vortex line density, and possesses considerable uncertainty. Taking $\chi_2 = 0.07L^{0.4}$ gives $\nu'/\kappa = 0.28\pm0.11$ for the high-density simulations, and $\nu'/\kappa = 0.33\pm0.20$ for the low-density ones.

We now turn to the second approach, in which we infer the diffusion coefficient from individual trajectories of diffusing tracers from time-averaged deviations [27] defined in Eq. (5). The typical temporal behavior of the rms deviation of tracers from their initial positions, $d_{\rm rms}$ vs t, averaged over 10 simulations, is shown in Fig. 2. The figure shows that the initially ballistic regime, $d_{\rm rms}\sim t$, is followed by a $d_{\rm rms}\sim t^{1/2}$ diffusive regime.

The effective diffusion coefficient ν', obtained from Eq. (4), is plotted as a function of time t in Fig. 3(a) (low-density simulations) and in Fig. 3(b) (high-density simulations; solid blue line). It is apparent that the effective diffusion settles down to the value $\nu'/\kappa\approx 0.5$ in both simulation sets. More precisely, we obtain $\nu'/\kappa = 0.526\pm0.064$ for low vortex line density and $\nu'/\kappa = 0.530\pm0.065$ for high vortex line density.

It is important to appreciate that, unlike the approach of Ref. [19], when we compute ν' via $d_{\rm rms}$, we do not include the tracers which belong to evaporating vortex loops as they move

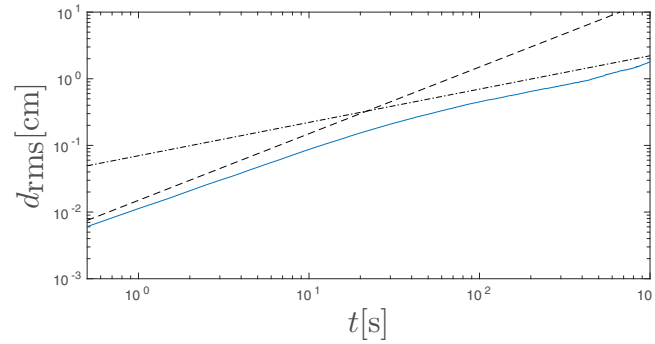

FIG. 2. Typical temporal dependence of the rms deviation of tracers from their initial position, $d_{\rm rms}$ (in cm) vs t (in s). Notice the transition from ballistic ($d_{\rm rms}\sim t$) to diffusive ($d_{\rm rms}\sim t^{1/2}$) regimes, indicated by the dashed and dot-dashed lines, respectively.

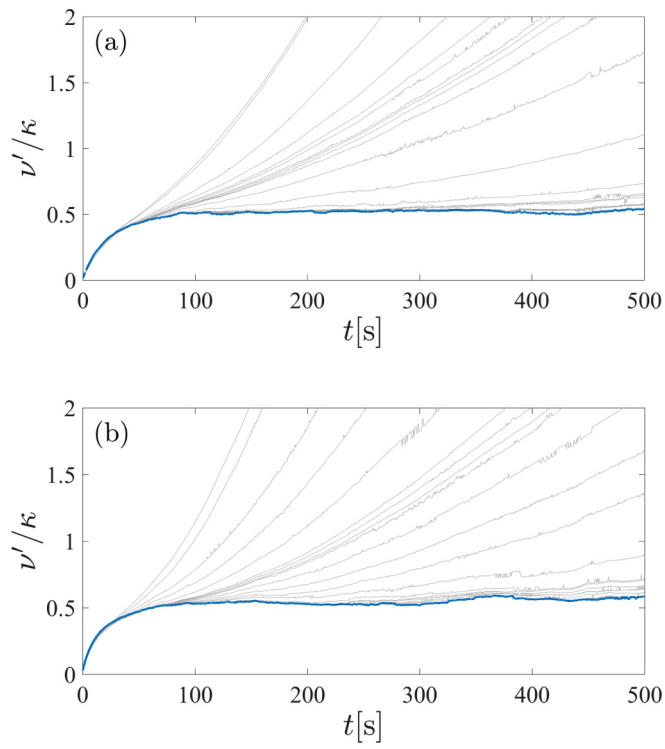

FIG. 3. Effective diffusion in units of the quantum of circulation, ν'/κ, vs time t (in s) (solid blue line) for (a) low-density simulations and (b) high-density simulations. Gray lines show the values of ν'/κ found as the minimum size of loops included in our calculation of $d_{\rm rms}$ is increased, from zero points (gray line which attains maximum value earliest) to 200 points, for which the value of ν'/κ found has converged.

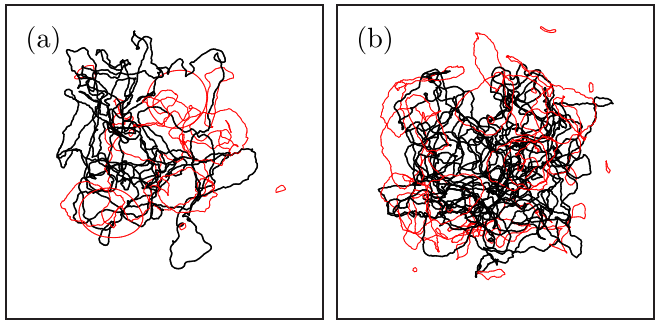

FIG. 4. Typical large knotted vortex structures (black lines) from simulations at (a) lower density [$L(|\mathbf{x}| = 0, t = 0) \sim 70$ cm^{-2}] and (b) higher density [$L(0,0) \sim 140$ cm^{-2}], at $t = 50$ s. The other vortex lines are shown as red curves.

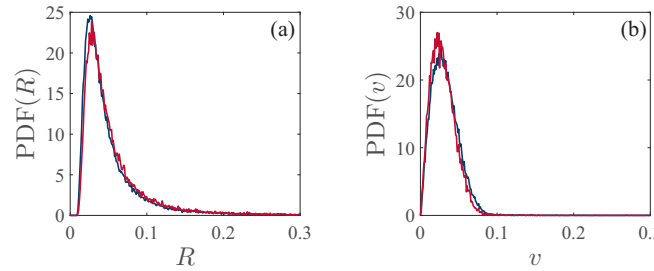

FIG. 5. Probability density functions (PDFs) of (a) the radius of curvature R and (b) velocity v of vortex filaments retained after disregarding loops containing fewer than 200 points. Red lines correspond to the lower-density simulations, blues lines to the higher-density simulations.

ballistically. The evaporating vortex loops, in fact, do not interact strongly with the other vortices of the cluster any longer, but move away with approximately constant speed determined by their average curvature. We observed an analogous effect in our previous 2D simulations [18], where vortex dipoles (the 2D analog of 3D vortex loops) ballistically evaporate from the vortex cluster. In this previous work we used a numerical procedure to identify and remove these fast moving dipoles from the calculation of ν'. Generalizing this 2D procedure to 3D, our analysis neglects fast evaporating vortex loops if they contain less than a certain critical number of discretization points N_c; in this way, we effectively set a minimum size for a vortex loop to be included in the calculation of $d_{\rm rms}$ and ν'. The critical number N_c is empirically determined. In Fig. 3 the gray lines show the values of ν'/κ found at increasing N_c, from $N_c = 0$ (gray line which attains maximum value earliest) to $N_c = 200$ (solid blue line); note that for $N_c = 200$ the value of ν'/κ has converged. This distinction between evaporating loops and the remaining vortex cluster is highlighted in Fig. 1, where vortex loops containing fewer than 200 discretization points (hence small compared with other loops) are shown in red, while the remaining vortex lines are shown in black.

We note that most of these large loops forming the vortex cluster and used in our analysis are not circular vortex rings but complex, often knotted vortex structures. Two such structures taken from two realizations are shown in Fig. 4 for illustration purposes. The two objects account for more than 54% [Fig. 4(a)] and more than 67% [Fig. 4(b)] of the total line length, and more than 80% [Fig. 4(a)] and more than 87% [Fig. 4(b)] of the total cluster line length retained in our analysis. The distributions of the local radius of curvature and local velocity of the loops retained in our analysis are shown in Fig. 5. Note that the peak radius of curvature, at around 0.025 cm, is considerably smaller than the radius of a circular ring consisting of 200 points at our chosen resolution ($\sim$0.64 cm), and the peak velocity is correspondingly higher. The local behavior of these structures is like that of far smaller vortex rings. Furthermore, if the collective behavior were ballistic, as for a system of isolated loops, we could expect vortices to drift by around 25 cm by 10^3 s, an order of magnitude greater than the deviation seen in Fig. 5.

Note that if we remove the evaporating loops from the analysis based on the modified Vinen equation (which the authors of Ref. [19] did not do), our estimate for ν' is (perhaps unsurprisingly) reduced. Indeed, without the evaporating loops, we obtain $\nu'/\kappa = 0.19 \pm 0.08$ in the higher-density simulations, and $\nu'/\kappa = 0.08 \pm 0.08$ in the lower-density ones.

IV. DISCUSSION

In conclusion, we have found that a cluster of turbulent vortex lines, initially localized in a region of space, spreads out driven by two effects: the evaporation of small vortex loops which leave the cluster, and the slower spread of the cluster itself. The latter effect can be modelled as a diffusion process which apparently emerges in this inviscid fluid context from the interaction between the vortex lines. By using the standard approach based on rms deviations, we have found that the effective diffusion coefficient, measured in units of the quantum of circulation κ, is $\nu'/\kappa \approx 0.5$, independently of the initial vortex line density. Our finding agrees quantitatively with values in the range $0.3 < \nu'/\kappa < 0.5$ obtained in a 2D trapped atomic Bose–Einstein condensate using the GPE model [18], keeping in mind that in these confined systems ν'/κ seems to be reduced by boundary effects (vortex images). It must be stressed that in both 2D and 3D, when determining the effective diffusion coefficient using the rms technique, we do not include the evaporating vortex loops because, unlike the vortices in the main cluster which undergo continual collisions, they move freely at constant speed.

Our results contrasts with the smaller value reported by Tsubota *et al.* [19], $\nu'/\kappa = 0.1$, which was obtained by fitting the solution of a modified Vinen equation. If we analyze our data with the modified Vinen equation we obtain a similar lower estimate for ν' but with significant error bars and sensitivity to the initial vortex line density; another drawback of this technique is that it requires independent knowledge of Vinen's parameter χ_2 as described in the Appendix. On the contrary, the technique based on the rms deviations of tracers' trajectories determines ν' more accurately and consistently and gives values comparable to previous findings in 2D.

It is also worth commenting on the difference between our initial conditions and the initial condition used in Ref. [19]. In Ref. [19], the vortex tangle was generated by a thermal counterflow using the local induction approximation. This

approximation in itself is known to be problematic in the presence of counterflow [32]; moreover a counterflow tangle is well known to be slightly anisotropic [32]. It seems plausible that this initial anisotropy in the initial condition used in Ref. [19] modifies the diffusion of the tangle. Indeed, a study on the effect of anisotropy on the diffusion of quantum vorticity could prove fruitful.

The theory of Nemirovskii [33] yields a value four times larger than ours, $\nu'/\kappa = 2.2$. This theory, as the modified Vinen equation, assumes (rather than infers) the existence of a diffusion process of vortex loops by postulating Brownian character of the vortex loops' dynamics. A superfluid's effective viscosity is also discussed in the different but related problem of the decay of superfluid turbulence, with experimental and numerical values [26,34–36] approximately in the range $0.01 < \nu'/\kappa < 1$ but more concentrated around 0.1.

Finally, we remark that the rms deviation method which we have used to estimate ν'/κ, being Lagrangian, could be used in future experimental studies of superfluid turbulence using the newly developed visualization techniques based on excited helium molecules [37–39].

ACKNOWLEDGMENT

C.F.B. acknowledges the support of EPSRC grant EP/R005192/1.

APPENDIX: DETERMINING χ_2

To estimate Vinen's parameter χ_2 at zero temperature and its dependence on the vortex line density L, we perform numerical simulations where identical vortex loops are continuously injected into a periodic box at random positions and orientations, at a constant rate. This gives us a known rate $L_{\rm Inj}$ at which the vortex line length is injected. The simulation is continued until a saturated value of L is achieved. When we are in this regime, the usual Vinen equation [40], which is usually written as

$$\frac{\partial L}{\partial t} = \chi_1 B \rho_n |v_{ns}| L^{3/2} - \frac{\kappa}{2\pi}\chi_2 L^2, \tag{A1}$$

where ρ_n is the normal fluid density, v_{ns} is the counterflow velocity, B is a mutual friction coefficient, and χ_1 and χ_2 are two dimensionless parameters, reduces to

$$0 = L_{\rm Inj} - \frac{\kappa}{2\pi}\chi_2 L^2, \tag{A2}$$

as we have a (statistically) steady value for the line density, and our loop injection replaces the usual finite-temperature source term from the normal fluid interacting with the vortex lines. This immediately gives $\chi_2 = \frac{2\pi L_{Inj}}{\kappa L^2}$. Repeating this procedure for a range of injection rates allows us to construct the plots shown in Fig. 6, from which we fit χ_2 as a function of L, finding $\chi_2 \approx 0.07 L^{0.4}$.

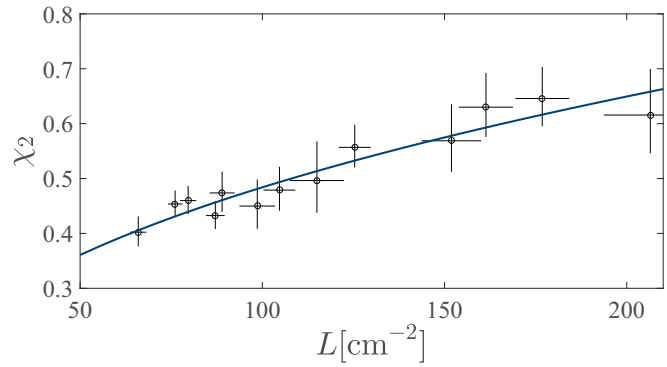

FIG. 6. Line density vs χ_2 calculated from steady-state simulations (black circles) with error bars showing one standard deviation, with fit in blue. Inset shows steady-state line density as a function of the injection rate, with fit in blue.

In a recent paper [26] a similar method is employed to estimate value of χ_2 at finite temperatures, using thermal counterflow as a source term. Values for χ_2 at 1.4 K (the lowest temperature reported) are reported as 2.10 ± 0.34 for $L = (3.59 \pm 0.34) \times 10^3$ cm^{-2}, 2.04 ± 0.19 for $L = (6.54 \pm 0.30) \times 10^3$ cm^{-2}, and 1.97 ± 0.13 for $L = (10.00 \pm 0.27) \times 10^3$ cm^{-2}. From our simulations we estimate $\chi_2 = 2.17$ for $L = 3.59 \times 10^3$, $\chi_2 = 2.79$ for $L = 6.54 \times 10^3$, $\chi_2 = 3.33$ for $L = 10.00 \times 10^3$. Our values are consistent to an order of magnitude, although slightly higher, possibly due to dissipation arising from the numerics. We note that, for small L, dissipation is dominated by Kelvin wave stimulated emission of phonons rather than by reconnections, so the assumption that dissipation scales as L^2 breaks down at some point, and accordingly our estimate of χ_2 for small L should be treated with caution.

[1] C. F. Barenghi, L. Skrbek, and K. R. Sreenivasan, Introduction to quantum turbulence, Proc. Natl. Acad. Sci. USA **111** (Suppl. 1), 4647 (2014).

[2] J. Salort, C. Baudet, B. Castaing, B. Chabaud, F. Davidaud, T. Didelot, P. Diribarne, B. Dubrulle, Y. Cagne, F. Gauthier, A. Girard, B. Hébral, B. Rousset, P. Thibault, and P.-E. Roche, Turbulent velocity spectra in superfluid flows, Phys. Fluids **22**, 125102 (2010).

[3] C. F. Barenghi, V. L'vov, and P.-E. Roche, Experimental, numerical and analytical velocity spectra in turbulent quantum fluid, Proc. Natl. Acad. Sci. USA **111** (Suppl. 1) 4683 (2014).

[4] C. F. Barenghi, Y. A. Sergeev, and A. W. Baggaley, Regimes of turbulence without an energy cascade, Sci. Rep. **6**, 35701 (2016).

[5] P. M. Walmsley and A. I. Golov, Quantum and Quasiclassical Types of Superfluid Turbulence, Phys. Rev. Lett. **100**, 245301 (2008).

[6] A. W. Baggaley, C. F. Barenghi, and Y. A. Sergeev, Quasiclassical and ultraquantum decay of superfluid turbulence, Phys. Rev. B **85**, 060501(R) (2012).

[7] E. Varga, J. Gao, W. Guo, and L. Skrbek, Intermittency enhancement in quantum turbulence, Phys. Rev. Fluids **3**, 094601 (2018).

[8] E. Rusaouen, B. Chabaud, J. Salort, and P.-E. Roche, Intermittency of quantum turbulence with superfluid fractions from 0% to 96%, Phys. Fluids **29**, 105108 (2017).

[9] L. Boué, V. L'vov, A. Pomyalov, and I. Procaccia, Enhancement of Intermittency in Superfluid Turbulence, Phys. Rev. Lett. **110**, 014502 (2013).

[10] M. S. Paoletti, M. E. Fisher, K. R. Sreenivasan, and D. P. Lathrop, Velocity Statistics Distinguish Quantum Turbulence from Classical Turbulence, Phys. Rev. Lett. **101**, 154501 (2008).

[11] A. W. Baggaley and C. F. Barenghi, Quantum turbulent velocity statistics and quasiclassical limit, Phys. Rev. E **84**, 067301 (2011).

[12] M. La Mantia and L. Skrbek, Quantum, or classical turbulence? Europhys. Lett. **105**, 46002 (2014).

[13] K. W. Schwarz and C. W. Smith, Pulsed-ion study of ultrasonically generated turbulence in superfluid ^{4}He, Phys. Lett. A **82**, 251 (1981).

[14] R. Hänninen and W. Schoepe, Universal critical velocity for the onset of turbulence of oscillatory superfluid flow, J. Low Temp. Phys. **153**, 189 (2008).

[15] M. J. Jackson, D. I. Bradley, A. M. Guénault, R. P. Haley, G. R. Pickett, and V. Tsepelin, Observation of quantum turbulence in superfluid ^{3}He-B using reflection and transmission of ballistic thermal excitations, Phys. Rev. B **95**, 094518 (2017).

[16] D. Schmoranzer, M. J. Jackson, V. Tsepelin, M. Poole, A. J. Woods, M. Človečko, and L. Skrbek, Multiple critical velocities in oscillatory flow of superfluid ^{4}He due to quartz tuning forks, Phys. Rev. B **94**, 214503 (2016).

[17] D. I. Bradley, R. P. Haley, S. Kafanov, M. T. Noble, G. R. Pickett, V. Tsepelin, J. Vonka, and T. Wilcox, Probing liquid ^{4}He with quartz tuning forks using a novel multifrequency lock-in technique, J. Low Temp. Phys. **184**, 1080 (2016).

[18] E. Rickinson, N. G. Parker, A. W. Baggaley, and C. F. Barenghi, Diffusion of quantum vortices, Phys. Rev. A **98**, 023608 (2018).

[19] M. Tsubota, T. Araki, and W. F. Vinen, Diffusion of an inhomogeneous vortex tangle, Physica B **329**, 224 (2003).

[20] K. W. Schwarz, Three-dimensional vortex dynamics in superfluid ^{4}He: Homogeneous superfluid turbulence, Phys. Rev. B **38**, 2398 (1988).

[21] C. F. Barenghi and N. G. Parker, *A Primer on Quantum Fluids* (Springer, Berlin, 2016).

[22] A. W. Baggaley, The sensitivity of the vortex filament method to different reconnection models, J. Low Temp. Phys. **168**, 18 (2012).

[23] W. F. Vinen, Mutual friction in a heat current in liquid helium II. III. Theory of mutual friction, Proc. R. Soc. A (London) **242**, 493 (1957).

[24] M. Tsubota, T. Araki, and S. K. Nemirovskii, Dynamics of vortex tangle without mutual friction in superfluid ^{4}He, Phys. Rev. B **62**, 11751 (2000).

[25] A. W. Baggaley and J. Laurie, Kelvin-wave cascade in the vortex filament model, Phys. Rev. B **89**, 014504 (2014).

[26] J. Gao, W. Guo, S. Yui, M. Tsubota, and W. F. Vinen, Dissipation in quantum turbulence in superfluid ^{4}He above 1 K, Phys. Rev. B **97**, 184518 (2018).

[27] G. Sikora, B. Krzysztof, and W. Agnieszka, Mean-squared-displacement statistical test for fractional Brownian motion, Phys. Rev. E **95**, 032110 (2017).

[28] A. Cidrim, A. C. White, A. J. Allen, V. S. Bagnato, and C. F. Barenghi, Vinen turbulence via the decay of multi-charged vortices in trapped Bose-Einstein condensates, Phys. Rev. A **96**, 023617 (2017).

[29] C. F. Barenghi and D. C. Samuels, Evaporation of a Packet of Quantised Vorticity, Phys. Rev. Lett. **89**, 155302 (2002).

[30] S. N. Fisher, A. J. Hale, A. M. Guénault, and G. R. Pickett, Generation and Detection of Quantum Turbulence in Superfluid ^{3}He-B, Phys. Rev. Lett. **86**, 244 (2001).

[31] G. W. Stagg, N. G. Parker, and C. F. Barenghi, Superfluid Boundary Layer, Phys. Rev. Lett. **118**, 135301 (2017).

[32] H. Adachi, S. Fujiyama, and M. Tsubota, Steady state of counterflow quantum turbulence: Vortex filament simulation with the full Biot-Savart law, Phys. Rev. B **81**, 104511 (2010).

[33] S. K. Nemirovskii, Diffusion of inhomogeneous vortex tangle and decay of superfluid turbulence, Phys. Rev. B **81**, 064512 (2010).

[34] P. Walmsley, D. Zmeev, F. Pakpour, and A. Golov, Dynamics of quantum turbulence of different spectra, Proc. Natl. Acad. Sci. USA **111**, 4691 (2014).

[35] S. Babuin, E. Varga. L. Skrbek, E. Leveque, and P.-E. Roche, Effective viscosity in quantum turbulence: A steady-state approach, Europhys. Lett. **106**, 24006 (2014).

[36] D. E. Zmeev, P. M. Walmsley, A. I. Golov, P. V. E. McClintock, S. N. Fisher, and W. F. Vinen, Dissipation of Quasiclassical Turbulence in Superfluid ^{4}He, Phys. Rev. Lett. **115**, 155303 (2015).

[37] D. N. McKinsey, W. H. Lippincott, J. A. Nikkel, and W. G. Rellergert, Trace Detection of Metastable Helium Molecules in Superfluid Helium by Laser-Induced Fluorescence, Phys. Rev. Lett. **95**, 111101 (2005).

[38] W. G. Rellergert, S. B. Cahn, A. Garvan, J. C. Hanson, and W. H. Lippincott, Detection and Imaging of He_2 Molecules in Superfluid Helium, Phys. Rev. Lett. **100**, 025301 (2008).

[39] W. Guo, J. D. Wright, S. B. Cahn, J. A. Nikkel, and D. N. McKinsey, Metastable Helium Molecules as Tracers in Superfluid ^{4}He, Phys. Rev. Lett. **102**, 235301 (2009).

[40] J. A. Geurst, Hydrodynamics of quantum turbulence in He II: Vinen's equation derived from energy and impulse of vortex tangle, Physica B (Amsterdam, Neth.) **154**, 327 (1989).